

1 Solid Lipid Nanoparticles for Image-Guided Therapy of 2 Atherosclerosis

3 Khalid Oumzil,^{†,‡} Michael A. Ramin,^{†,‡} Cyril Lorenzato,[§] Audrey Hémadou,[§] Jeanny Laroche,[§]
4 Marie Josée Jacobin-Valat,[§] Stephane Mornet,^{||} Claude-Eric Roy,^{†,‡} Tina Kauss,^{†,‡} Karen Gaudin,^{†,‡}
5 Gisèle Clofent-Sanchez,[§] and Philippe Barthélémy*,^{†,‡}

6 [†]University of Bordeaux, ARNA laboratory, F-33000 Bordeaux, France

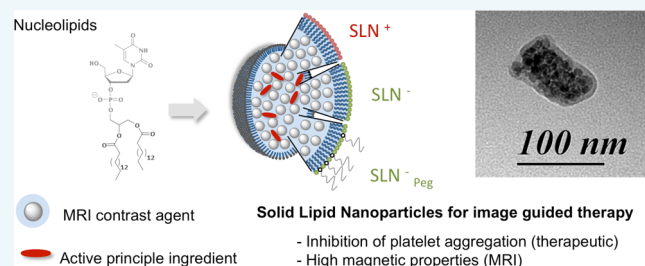
7 [‡]INSERM, U869, ARNA laboratory, F-33000 Bordeaux, France

8 [§]CRMSB Centre de Résonance Magnétique des Systèmes Biologiques, UMR 5536, CNRS, University of Bordeaux, F-33076
9 Bordeaux, France

10 ^{||}Institut de Chimie de la Matière Condensée de Bordeaux, ICMCB UPR CNRS 9048, University of Bordeaux, F-33608 Pessac,
11 France

12 **S** Supporting Information

13 **ABSTRACT:** Although the application of nanotechnologies
14 to atherosclerosis remains a young field, novel strategies are
15 needed to address this public health issue. In this context, the
16 magnetic resonance imaging (MRI) approach has been
17 gradually investigated in order to enable image-guided
18 treatments. In this contribution, we report a new approach
19 based on nucleoside-lipids allowing the synthesis of solid lipid
20 nanoparticles (SLN) loaded with iron oxide particles and
21 therapeutic agents. The insertion of nucleoside-lipids allows
22 the formation of stable SLNs loaded with a prostacycline
23 (PGI₂) able to inhibit platelet aggregation. The new SLNs feature better relaxivity properties in comparison to the clinically used
24 contrast agents Feridex, indicating that SLNs are suitable for image-guided therapy.



25 **■** INTRODUCTION

26 Atherosclerosis is one of the leading causes of death in the
27 developed countries. While the search for efficient treatments
28 continues, it becomes clear that the implementation of new
29 tools combining diagnostic with therapeutic approaches should
30 play an essential role in formulating effective treatment
31 plans.¹⁻⁵ Nanoparticles have the ability to carry various
32 therapeutic and/or imaging agents.^{6,7} In this regard, theranos-
33 tic,⁸⁻¹⁰ which combines diagnostic and therapeutic modalities
34 into a single nanosized carrier, has recently emerged as a
35 potential tool for atherosclerosis imaging¹¹ and treatment.¹²
36 Monitoring disease progression and response to therapy can be
37 followed by magnetic resonance imaging (MRI), which is a
38 noninvasive imaging and diagnostic technique used worldwide
39 in numerous laboratories. This technique is very efficient for
40 imaging soft tissues and provides detailed anatomical images of
41 the body. Ultrasmall superparamagnetic iron oxide (USPIO)
42 particles are maghemite or magnetite nanoparticles currently
43 used as contrast agent in magnetic resonance imaging.¹³
44 Several promising theranostic systems are currently under
45 investigation and most of these systems involve micelles,
46 liposomes, or polymer-based materials.¹⁴⁻¹⁸ Surprisingly, solid
47 lipid nanoparticles (SLN)^{19,20} loaded with iron oxide nano-
48 particles have been poorly investigated.

Herein, we report the first example of an SLN featuring both 49
multiple maghemite nanoparticles and an active principle 50
ingredient (API) stabilized by nucleoside-lipids.^{21,22} It is 51
noteworthy that the nucleoside lipids, or nucleolipids, used in 52
these formulations allow the formation of stable SLNs (Figure 53
1), whereas these nano-objects cannot be obtained using lipids. 54
A nanoprecipitation procedure was used to generate the SLN 55
loaded with both maghemite nanoparticles and an API such as 56
 α -tocopherol or prostacyclin PGI₂. The inhibition of platelet 57
activation and aggregation by SLN loaded with prostacyclin was 58
evaluated with the aim of developing a new theranostic tool 59
against atherosclerosis. 60

61 **■** RESULTS AND DISCUSSION

In a first series of experiments, α -tocopherol was selected as 62
hydrophobic API in order to evaluate the drug loading 63
capability of the SLN. Accordingly, a nucleolipid mixed with 64
 α -tocopherol and iron oxide nanoparticles dissolved in ethylic 65
ether was added dropwise to water under stirring. This simple 66
procedure allows the spontaneous formation of the SLNs. In 67
order to investigate the influence of the chemical structure of 68

Received: October 30, 2015

Revised: December 24, 2015

SLNs / Formulations with nucleolipids

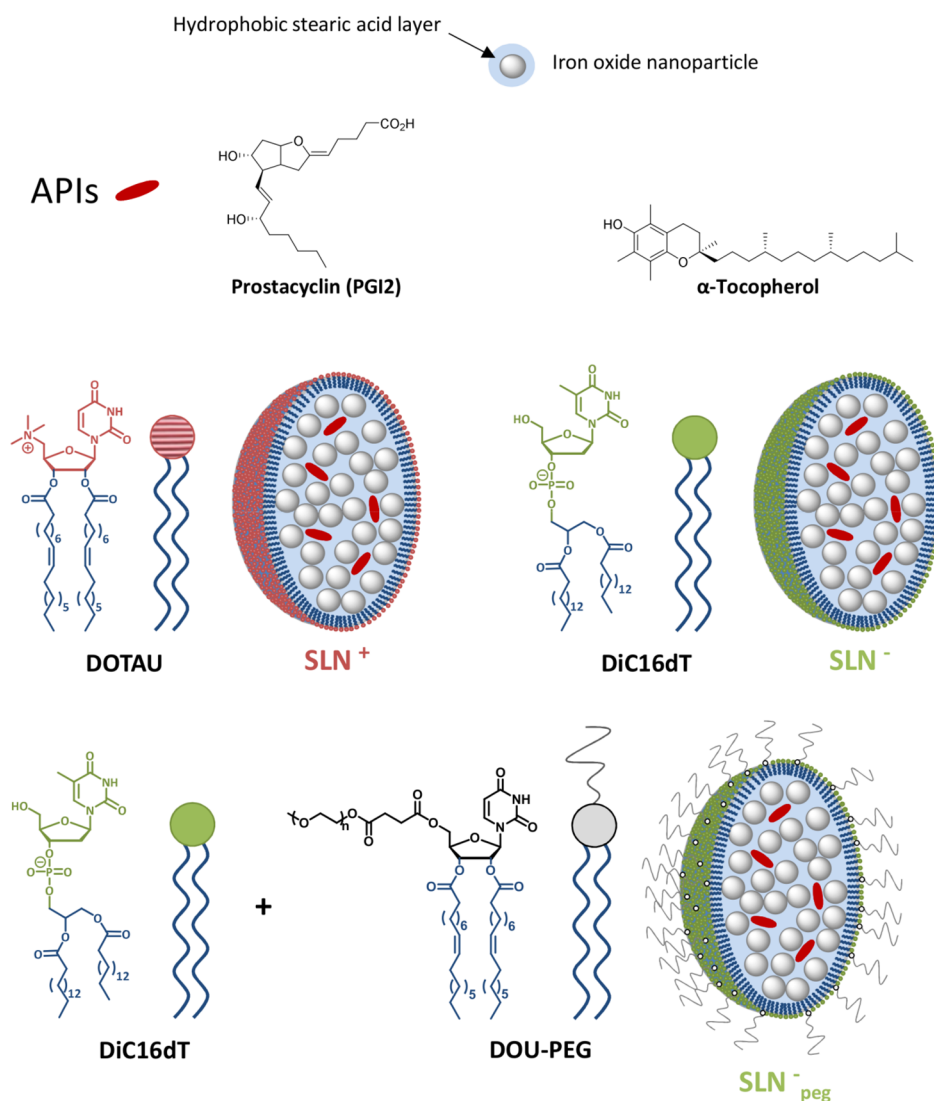


Figure 1. Nucleolipids (diC16dT: Thymidine 3'-(1,2-dipalmitoyl-*sn*-glycero-3-phosphate; DOTAU: *N*-[5'-(2',3'-dioleoyl)uridine]-*N*',*N*',*N*'-trimethylammonium; DOU-PEG: 5'-(*O*-Methyl-*O*'-succinylpolyethylene glycol)-2',3'-dioleoyluridine), API, and maghemite used for the implementation of the solid lipid nanoparticles (SLN). SLNs are lipid-based nanocarriers encapsulating grapes of ultrasmall superparamagnetic iron oxide (USPIO) particles and APIs (α -tocopherol or prostacyclin PGI2).

69 nucleolipids on the nanocarrier stability, we synthesized SLNs
70 (Figure 1) featuring either positive (SLN⁺ and SLN⁺_{Toco}) or
71 negative charges (SLN⁻, SLN⁻_{peg}, SLN⁻_{peg/PGI2}).

72 **Physicochemical Studies.** Dynamic light scattering (DLS)
73 experiments were carried out to confirm the formation of SLNs.
74 Both positive and negative nucleolipids (DOTAU and
75 diC16dT) form similar grapes of nanoparticles in aqueous
76 solution with reasonably narrow polydispersity (PDI = 0.175
77 and 0.225; diameter = 80 and 98 nm, respectively, Figure 2c).
78 As expected, the zeta potentials of SLN based objects depend
79 on the nucleolipid polar heads (ζ = +55 and -27 mV for SLN⁺
80 and SLN⁻). Importantly, a control experiment achieved in the
81 absence of nucleolipid led to the formation of a precipitate,
82 demonstrating that nucleobases are needed to stabilize the
83 SLNs (see Figure S19). Indeed, it is hypothesized that
84 internucleobase stacking plays an important role in stabilizing
85 the SLN structures. To confirm the base-stacking interactions
86 in the nano-objects, we measured the UV spectra of diC16dT

self-assemblies and thymidine in water at room temperature. 87
The molar absorptivity, ϵ , at 261 nm for the diC16dT self- 88
assemblies is 3.4 mM⁻¹ cm⁻¹ compared with that for thymidine 89
(ϵ = 6 mM⁻¹ cm⁻¹). This hypochromic effect indicates a 90
different organization of the nucleoside in the nucleolipid self- 91
assemblies compared with thymidine dissolved in water, 92
supporting a stacking arrangement of the pyrimidine bases. 93

The presence of polyethylene glycol (Peg) moieties on the 94
surface of nanocarriers has been shown to extend blood- 95
circulation time while diminishing mononuclear phagocyte 96
system uptake (stealth nanosystems).^{2,3} Hence, SLNs featuring 97
Peg on the surface were synthesized using diC16dT and DOU- 98
PEG. This mixture provides stealth pegylated grapes (SLN⁻_{peg}) 99
of 92 nm in diameter and a zeta potential of -23.6 mV (Figures 100
S17 and S18). SLNs loaded with different APIs were 101
synthesized. Accordingly, the nanocarriers formulated with 102
cationic nucleolipid DOTAU²⁴ and α -tocopherol (SLN⁺_{Toco}) 103
exhibit a size of 108 nm in diameter and a zeta potential of 104

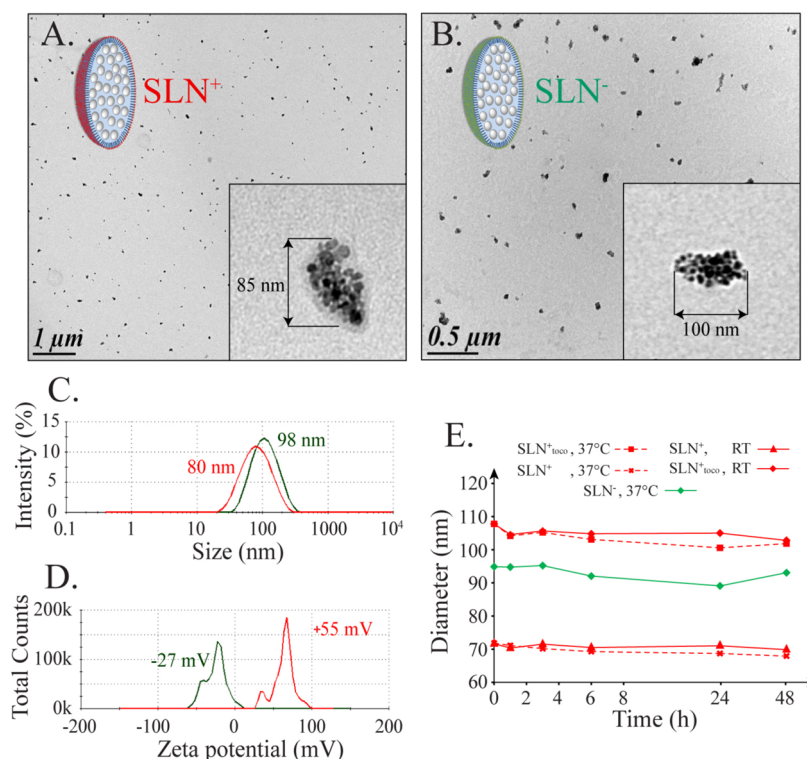


Figure 2. TEM images and schematic representations showing grapes of nanoparticles stabilized either with DOTAU (SLN⁺, A) or diC16dT (SLN⁻, B). Inset corresponds to a magnification of the TEM images. (C) Size distribution of the SLN⁺ (red) and SLN⁻ (green). (D) Zeta potential of SLN⁺ (red) and SLN⁻. (E) Colloidal stability versus time at RT and 37 °C.

105 +49.2 mV (Figures S110 and S111). *In fine*, pegylated grapes
 106 (loaded with prostacyclin (PGI₂)) were synthesized using
 107 diC16dT and DOU-PEG as nucleolipids (SLN⁻_{Peg/PGI₂}).
 108 SLN⁻_{Peg/PGI₂} show a diameter of 154 nm and a ζ of -22.6
 109 mV (Figures S113 and S114).

110 Transmission electron microscopy (TEM) images of the
 111 SLNs were captured (Figure 2A,B). In agreement with the DLS
 112 data, both positive and negative nucleolipids self-assemble into
 113 similar nano grapes in the presence of iron oxide nanoparticles.
 114 Interestingly, similar grapes were observed for different SLNs
 115 loaded with APIs (see Figures S13, S16, and S112, for example).

116 The colloidal stability of SLNs was studied by monitoring the
 117 diameter of grapes versus time. The kinetics at room
 118 temperature and 37 °C are shown on Figure 2E. The size of
 119 all SLNs are not modified for more than 2 days at both room
 120 temperature and 37 °C indicating that these nano-objects may
 121 be suitable for theranostic applications.

122 Next we evaluated the drug loading capabilities of the novel
 123 formulations. A reverse phase UHPLC method was developed
 124 for nucleolipids and α -tocopherol quantification from the SLN
 125 composition containing iron oxide nanoparticles. For example,
 126 this method allows the separation of the DOTAU and the
 127 SLN⁺ components within 5 min. Quantification of both
 128 DOTAU and α -tocopherol was then possible, which led to
 129 the determination of the loading ratios and encapsulation
 130 yields. Accordingly, in the case of SLN⁺_{Toco} a loading ratio and
 131 an encapsulation yield of 42% and 10% were obtained,
 132 respectively.

133 **Magnetic Properties of the SLNs.** In order to determine
 134 whether the nucleolipids based SLNs could be used as MRI
 135 contrast agents; we measured the longitudinal (r_1) and
 136 transverse (r_2 and r_2^*) relaxivities of the SLNs. Figure 3 shows
 137 the transverse relaxation rates (R_2^*) of the SLN⁻ and SLN⁺

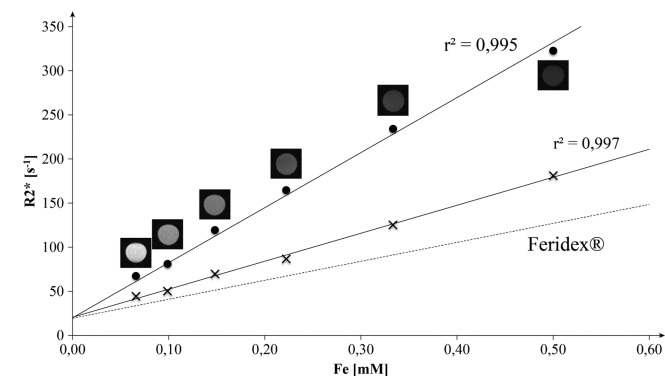


Figure 3. Magnetic resonance relaxometry of SLN⁻ and SLN⁺ at 4.7 T. Transverse relaxation rates (R_2^*) versus iron concentration for the SLN⁻ (●) with their corresponding T_1 -weighted MRI at TE = 3.5 ms and SLN⁺ (×). Linear regression fit was used to extract the relaxivities (solid lines).

138 samples as a function of iron concentration. The theoretical R_2^*
 139 of the clinically used contrast agents Feridex was plotted for
 140 comparison.²⁵ Both SLN⁻ and SLN⁺ dispersions have higher
 141 magnetic properties than those shown by Feridex at the same
 142 iron concentrations. Importantly, compared to Feridex ($r_2^* =$
 143 215) the SLN⁻ and SLN⁺ give higher contrast enhancement in
 144 MRI as revealed by the relaxivities measured at 4.7 T ($r_2^* =$
 145 557 and 317 s⁻¹ mM⁻¹, respectively; see Table S11).

Inhibition of Platelet Aggregation. Atherosclerosis is a
 146 chronic disease of coronary, intracranial, and peripheral arterial
 147 diseases, which together account for one of the leading causes
 148 of death worldwide. Experimental and clinical studies have
 149 shown the possibilities of treating atherosclerosis by bypassing
 150 the common method using lipid-lowering drugs. More recent
 151

152 investigations have focused on new classes of nanoparticles
 153 capable of detecting²⁶ and/or counteracting plaque develop-
 154 ment by acting on the components involved in initiating
 155 atherogenesis such as modulators of biologically active lipids,
 156 renin-angiotensin-aldosterone system, oxidative stress, and
 157 macrophage cholesterol efflux.^{27–29} These investigations have
 158 been offering new directions in the therapeutic and preventive
 159 fields of atherosclerosis. Among biologically active lipids,
 160 prostacyclin (PGI₂), a major product of COX-2 catalyzed
 161 metabolism of arachidonic acid, is a naturally occurring
 162 prostaglandin with two potent pharmacological actions: (1)
 163 direct vasodilatation of pulmonary and systemic arterial vascular
 164 beds, and (2) inhibition of platelet aggregation. Several studies
 165 have demonstrated that PGI₂ protects against atherothrombo-
 166 sis. Arehart et al. demonstrated that patients harboring a
 167 dysfunctional human prostacyclin receptor variant (R212C)
 168 exhibited an enhanced atherothrombotic phenotype.³⁰ The
 169 recent withdrawal of rofecoxib, a selective COX-2 inhibitor, due
 170 to increased cardiovascular events further supports the critical
 171 role of prostacyclin in inhibiting atherothrombosis in
 172 humans.^{31,32} Multiple mechanisms are likely to be involved in
 173 the effects of prostaglandins and their receptors on
 174 atherosclerosis, including control of platelet activation and
 175 aggregation, lipid peroxidation, and leukocyte recruitment into
 176 the vessel wall. The huge presence of platelets within the intima
 177 of atheroma was recently demonstrated, adding more value to
 178 the interest of blocking platelet aggregation for therapeutic
 179 purposes.³³ To determine whether SLNs involving both API
 180 and an MRI contrast agent would be suitable for atherosclerosis
 181 therapy, we examined the effect of SLN loaded with
 182 prostacyclin on platelet aggregation. In this work PGI₂ was
 183 incorporated into diC16dT based SLN⁻ (SLN⁻_{Peg/PGI₂}; see SI)
 184 and activity of PGI₂ further tested by aggregometry.
 185 Aggregometry experiments measure the ability of various
 186 agonists to platelet-rich plasma (PRP) to induce in vitro
 187 platelet activation and platelet-to-platelet aggregation. PGI₂
 188 analogues can be hydrolyzed at neutral pH in blood and are
 189 also subject to enzymatic degradation.³⁴ Thus, PRP has been
 190 incubated with SLN⁻_{Peg/PGI₂} for 15 min and 3 h to evaluate the
 191 maintenance of PGI₂ activity. The drug encapsulated in
 192 SLN⁻_{Peg/PGI₂} loaded with iron oxide was able to totally inhibit
 193 the aggregation of platelets induced by adenosine 5'-
 194 diphosphate (ADP) and thrombin receptor-activating peptide-
 195 6 (TRAP-6) at 15 min and 3 h incubation, whereas SLN
 196 without API showed a complete aggregation (Figure 4).
 197 Effective PGI₂ content of SLNs was estimated between 25
 198 and 50 ng/mL (see Figure SI15). These preliminary experi-
 199 ments are of high interest to demonstrate that the activity of
 200 PGI₂ is preserved in SLN nanoparticles.

201 ■ CONCLUSION

202 In this study, we have shown that nucleolipids featuring
 203 positive, negative, or neutral polar heads allow for the formation
 204 of solid lipid nanoparticles (SLNs) loaded with iron oxide
 205 particles and therapeutic agents. Importantly, SLNs cannot be
 206 synthesized in the absence of nucleolipids, indicating that the
 207 nucleobases are contributing to the stabilization of the grapes.
 208 Compared to the clinically used contrast agents Feridex, the
 209 SLNs have higher magnetization properties with 2.6-fold higher
 210 transverse relaxivity at 4.7 T. It is noteworthy that the insertion
 211 of the fragile PGI₂ into the SLNs maintains its bioactivity as
 212 shown by a complete inhibition of platelet aggregation.
 213 Altogether these results indicate that this strategy, added to

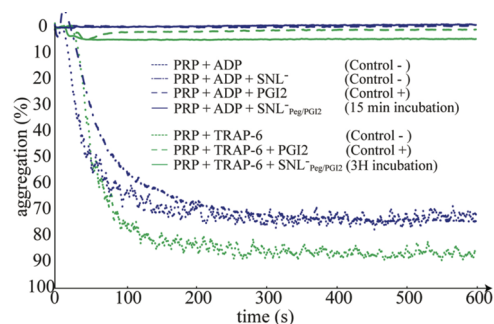


Figure 4. Inhibition of platelet aggregation by SLN⁻_{Peg/PGI₂}. The percentage of aggregation was followed versus time. PRP (207 μ L) was stirred in cuvettes at 37 $^{\circ}$ C and agonists ADP (blue curves) or TRAP-6 (green curves) were added at 5 s to promote platelet aggregation. SLN⁻_{Peg/PGI₂} (solid lines) as well as free PGI₂ totally inhibit the platelet aggregation induced by both ADP (15 min incubation) and TRAP-6 (3 h incubation) agonists, whereas SLN⁻ nanoparticles, used as negative control (dot-dash line), show complete ADP aggregation.

an antibody-guided addressing scheme, may allow for
 constructing nanoparticle grapes suitable for theranostic
 purposes in the field of atherosclerosis.

■ EXPERIMENTAL PROCEDURES

Preparation of Iron Oxide Nanoparticles Clusters Encapsulated by Nucleolipids. *Synthesis of SLN⁺ (Encapsulation of Iron Oxide Nanoparticles Clusters by DOTAU).* 100 μ L of stock solution of positively charged nucleolipid (DOTAU) (50 mg/mL in chloroform) and 20 μ L of stock solution of iron oxide nanoparticles coated with stearic acid (10 mg/mL in ether) were mixed. DOTAU was prepared according to Chabaud et al.²⁵ The organic phase was added dropwise into the aqueous phase (2 mL of Milli-Q Water) placed in a glass tube under stirring by vortex. Then the mixture was placed in a glass flask. Ether was removed under vacuum and the resulting crude material solution was sonicated 3 times (3 \times 15 min) and purified on LS columns to give a pure solution of nanoparticles. The size distribution by intensity measured by dynamic light scattering (DLS) ($d = 80$ nm) and the zeta potential distribution measured with a 25 MalvernNanoZS device (zeta potential = +55 mV) are shown in Figures SI1 and SI2.

Synthesis of SLN⁻ (Encapsulation of Iron Oxide Nanoparticles Clusters by diC16dT). 75 μ L of stock solution of negatively charged nucleolipid (diC16dT) (50 mg/mL in chloroform), 25 μ L of stock solution of 1,2-dioleoyl-*sn*-glycero-3-5 Phosphocholine (DOPC) (Avanti Polar lipids, 50 mg/mL in chloroform) and 20 μ L of stock solution of iron oxide nanoparticles (10 mg/mL in chloroform) were mixed. DiC16dT was prepared as reported by Khaty et al.³⁶ The organic phase was added dropwise into the aqueous phase (2 mL of Milli-Q Water) placed in a glass tube under stirring by vortex. Then, the mixture was placed in a glass flask. Chloroform was removed under vacuum and the resulting crude material solution was sonicated 3 times (3 \times 15 min) and purified on LS columns to give pure solution of nanoparticles. The size distribution by intensity measured by DLS ($d = 98$ nm) and the zeta potential distribution measured with a 25 MalvernNanoZS device (zeta potential = -27 mV) are shown in Figures SI4 and SI5.

Synthesis of SLN⁻_{peg} (Encapsulation of Iron Oxide Nanoparticles Clusters by diC16dT). 75 μ L of stock solution of negatively charged nucleolipid (diC16dT) (50 mg/mL in 255

256 chloroform), 25 μL of stock solution of 1,2-dioleoyl-*sn*-glycero-
257 3–5 phosphocholine (DOPC) (Avanti Polar lipids, 50 mg/mL
258 in chloroform), 30 μL of stock solution of neutral nucleolipid
259 (DOU-PEG2000) (10 mg/mL in chloroform), and 20 μL of
260 stock solution of iron oxide nanoparticles (10 mg/mL in
261 chloroform) were mixed. DiC16dT was prepared as reported
262 by Khiaty et al.³⁶ DOU-PEG2000 was prepared according to
263 Oumzil et al.³⁵ The organic phase was added dropwise into the
264 aqueous phase (2 mL of Milli-Q Water) placed in glass tube
265 under stirring by vortex. Then, the mixture was placed in a glass
266 flask. Chloroform was removed under vacuum and the resulting
267 crude material solution was sonicated 3 times (3×15 min) and
268 purified on LS columns to give pure solution of nanoparticles.
269 The size distribution by intensity measured by DLS ($d = 92$
270 nm) and the zeta potential distribution measured with a
271 MalvernNanoZS device (zeta potential = -23.6 mV) are shown
272 on Figures S17 and S18.

273 **Control (DOPC with Iron Oxide Nanoparticles).** 100 μL of
274 stock solution of 1,2-dioleoyl-*sn*-glycero-3–5 phosphocholine
275 (DOPC) (Avanti Polar lipids, 50 mg/mL in chloroform) and
276 20 μL of stock solution of iron oxide nanoparticles (10 mg/mL
277 in chloroform) were mixed. The organic phase was added
278 dropwise into the aqueous phase (2 mL of Milli-Q Water)
279 placed in glass tube under stirring by vortex. Then the mixture
280 was placed in glass flask. Chloroform was removed under
281 vacuum and the resulting crude material solution was sonicated
282 3 times (3×15 min). The iron oxide nanoparticles are not
283 stable in aqueous solution and precipitate (Figure S19).

284 **Preparation of Iron Oxide Nanoparticles Clusters with**
285 **Nucleolipid and API.** *Synthesis of $\text{SLN}^+_{\text{Toco}}$ (Preparation of*
286 *a DOTAU Based Nanocarrier Composition Containing Iron*
287 *Oxide Nanoparticles and α -Tocopherol).* 100 μL of stock
288 solution of positively charged nucleolipid (DOTAU) (50 mg/
289 mL in ether), 10 μL of stock solution of α -tocopherol (Sigma-
290 Aldrich, 50 mg/mL in ether), and 20 μL of stock solution of
291 iron oxide nanoparticles (10 mg/mL in ether) were mixed. The
292 organic phase was added dropwise into the aqueous phase (2
293 mL of Milli-Q Water) placed in a glass tube under stirring by
294 vortex. Then, the mixture was placed in a glass flask. Ether was
295 removed under vacuum and the resulting crude material
296 solution was sonicated for 3×15 min and purified on LS
297 columns to give pure solution of nanoparticles. The size
298 distribution by intensity measured by DLS ($d = 108$ nm) and
299 the zeta potential distribution measured with a MalvernNanoZS
300 device (zeta potential = $+49.2$ mV) are shown on Figures S110
301 and S111.

302 *Synthesis of $\text{SLN}^-_{\text{Peg/PGI2}}$ (Preparation of a Lipid-Based*
303 *(diC16dT, DOPC, and DOU-PEG2000) Nanocarrier Compo-*
304 *sition Containing Iron Oxide Nanoparticles and Prostacyclin*
305 *(PGI2.Na).* 75 μL of stock solution of negatively charged
306 nucleolipid (diC16dT) (50 mg/mL in chloroform + 2% Et_3N),
307 25 μL of stock solution of DOPC (50 mg/mL in chloroform
308 + 2% Et_3N), 30 μL of stock solution of neutral nucleolipid
309 (DOU-PEG2000) (10 mg/mL in chloroform + 2% Et_3N), 1 mg
310 of PGI2.Na (Sigma-Aldrich), and 20 μL of stock solution of
311 iron oxide nanoparticles (10 mg/mL in chloroform + 2% Et_3N)
312 were mixed. The organic phase was added dropwise into the
313 aqueous phase (2 mL of carbonate–bicarbonate buffer, pH 9.6
314 at 25 C) placed in glass tube under stirring by vortex. Then the
315 mixture was placed in a glass flask. Chloroform was removed
316 under vacuum and the resulting crude material solution was
317 sonicated for 3×15 min and purified on LS column to give a
318 pure solution of nanoparticles. The size distribution by

intensity measured by DLS ($d = 154$ nm) and the zeta 319
potential distribution measured with a MalvernNanoZS device 320
(zeta potential = -22.6 mV) are shown on Figures SI13 and 321
SI14. 322

Stability Study. Iron oxide nanoparticle clusters encapsu- 323
lated by DOTAU (SLN^+) or diC16dT (SLN^-) and DOTAU- 324
based nanocarrier composition comprising iron oxide nano- 325
particles and α -tocopherol ($\text{SLN}^+_{\text{Toco}}$) in 500 μL of Milli-Q 326
water were incubated at 37 $^\circ\text{C}$ under a 500 rpm stirring. For 327
different times (0, 1, 3, 6, 24, 48 h), particle sizes were 328
determined using a Zetasizer 3000 HAS MALVERN. The 329
results show that the overall sizes, either in the absence or in 330
the presence of therapeutic agents, and either positively or 331
negatively charged, are not modified as a function of time 332
(more than 2 days), which indicates colloidal stability both at 333
room temperature and at 37 $^\circ\text{C}$ (see SI). 334

Preparation of Samples for HPLC Analysis and Dosage of 335
DOTAU and α -Tocopherol (SLN^+ and $\text{SLN}^+_{\text{Toco}}$). Pure 336
suspensions of cationic nanoparticles prepared were centrifuged 337
at 14 000 rpm for 15 min in order to remove the supernatant. 338
Cationic nanoparticles (in the form of a pellet) were suspended 339
in ethanol. The resulting solution was mixed for 15 min at RT 340
and centrifuged at 14 000 rpm for 5 min. The supernatant was 341
evaporated and then solubilized in 5 mL of mobile phase follow 342
by a 5 \times dilution before injection in HPLC (Figure SI18A and 343
B). The precipitate was analyzed by HPLC after solubilization 344
in 5 mL of mobile phase (Figure SI18C and D). A reverse 345
phase UHPLC method was developed for nucleolipid 346
(DOTAU) and α -tocopherol quantification from the lipid- 347
based nanocarrier composition containing iron oxide nano- 348
particles. This method allows the separation of the DOTAU 349
and API within 5 min for lipid-based (DOTAU) nanocarrier 350
composition. The separation was carried out with a column 351
Syncronis C18 50 \times 2.1 mm, 1.7 μm with a mobile phase 352
composed of MeOH + 0.1% HCOOH. The flow rate was set to 353
0.2 mL/min. The detection was performed at 293 and 260 nm 354
for α -tocopherol and DOTAU, respectively. The injected 355
volume was 1.0 μL , which allowed the detection of DOTAU 356
and α -tocopherol at limit of quantification of 5 ng and 15 ng 357
respectively. Standard curves for DOTAU and α -tocopherol, as 358
shown on Figures SI15 and SI16, were generated by 359
determining the intensity of signal versus concentrations. The 360
HPLC analyses are shown in Figure SI18A–D. Figure SI18A 361
and B present supernatant analysis and C and D precipitate 362
analysis. Quantification of both DOTAU and α -tocopherol was 363
then possible, which led to encapsulated recovery and 364
determination of loading ratio values. Loading ratio was 42%; 365
that obtained in the case of a DOTAU/ α -tocopherol with a 366
ratio 10:1 for processing and the encapsulated drug recovery 367
was around 10%. 368

MR Relaxometry. A total number of 8 different concentra- 369
tions ranging from 0 to 0.5 mM Fe of both SLN^+ and SLN^- 370
were prepared in Eppendorf PCR Tubes (0.5 mL). Transverse 371
images passing through the 8 tubes were acquired on a 4.7 T 372
Bruker Biospin (Billerica, MA) MRI system with a 1H whole 373
body RF volume coil of 35 mm inner diameter and the 374
relaxation rate (R_n) maps were computed using the Paravision 375
6.0 software. Samples were scanned at 21 $^\circ\text{C}$ with a 256 \times 192 376
matrix and a FOV = 40 \times 30 mm. R_1 measurements were 377
acquired using the Bruker T_1 map RARE method (TR = 5000, 378
3000, 1500, 800, 400, 200 ms; TE = 6 ms; RARE factor = 2). 379
Multi-spin–echo ($\Delta\text{TE} = 8.45$; number of echoes = 20; TR = 2 380
s) and gradient-echo (flip angle = 60° ; number of echo = 8 ; TE 381

382 initial = 3.5 ms; $\Delta TE = 5$ ms; TR = 800 ms; flyback) sequences
383 were employed to compute an R_2 map and R_2^* map,
384 respectively. The mean relaxation rates, R_n , of each dilution
385 were calculated from ROIs encompassing each tube and plotted
386 versus their corresponding Fe concentrations. A linear
387 regression was used to extract the relaxivity (r_n) of each
388 sample, given as the slope of the resulting line in units of s^{-1}
389 mM^{-1} of Fe.

390 **Analysis of Bioactivity of Encapsulated API.** Blood was
391 obtained in a 1/10th volume of 3.8% sodium citrate from
392 healthy volunteers who had not taken any drugs known to
393 affect platelet function for 2 weeks prior to the study. Platelet-
394 rich plasma (PRP) is prepared by centrifugation at 20 °C for
395 10–15 min at 150–200g and stored at room temperature.
396 Platelet-poor plasma (PPP) is prepared by further centrifuga-
397 tion of the remaining plasma at 2700g for 15 min and calibrates
398 the 100% light transmission of the aggregometer. PRP (207
399 μL) was stirred in cuvettes at 37 °C and platelet agonists (ADP
400 (10 μM) or TRAP-6 (100 μM) were added at 5 s to promote
401 platelet aggregation. The in vitro platelet aggregation was
402 determined using a four-channel light transmission aggreg-
403 ometer (APACT 4004, ELITech, France).

404 **Transmission Electronic Microscopy (TEM).** Nanoparticles
405 were visualized by negative staining microscopy. 10 μL aliquots
406 of nanoparticles (1 mM) were transferred to a carbon-coated
407 copper grid for 10 min. The sample was then dried and stained
408 with 2.5% (W/W) of uranyl acetate in water for 5 min. The
409 specimens were observed with a Hitachi H 7650 electron
410 microscope.

411 **Particle Size and Zeta Determination.** Particle zeta and size
412 were determined using a Zetasizer 3000 HAS MALVERN.
413 Experiments were realized with 50 μL of the nanoparticles
414 diluted in 1.2 mL of DI water and measurements were
415 performed at 25 °C.

416 ■ ASSOCIATED CONTENT

417 ● Supporting Information

418 The Supporting Information is available free of charge on the
419 ACS Publications website at DOI: 10.1021/acs.bioconj-
420 chem.5b00590.

421 DLS data, zeta potentials and TEM of SLNs synthesized
422 in different experimental conditions, HPLC dosages, and
423 MR relaxometry (PDF)

424 ■ AUTHOR INFORMATION

425 Corresponding Author

426 *E-mail: philippe.barthelemy@inserm.fr.

427 Notes

428 The authors declare no competing financial interest.

429 ■ ACKNOWLEDGMENTS

430 This work has been supported by two public grants of the
431 French National Agency (ANR) (1) in the frame of the
432 Investments for the Future Program, referenced ANR-10-
433 LABX-57 and named TRAIL (Translational Research and
434 Advanced Imaging Laboratory) MIMATHUMAB and (2)
435 within the context of SVE5 program, named ATHERANOS.
436 The authors thank the Bordeaux Imaging Centre (BIC) for
437 technical assistance during TEM observations.

■ REFERENCES

- 438
439 (1) Libby, P., Ridker, P. M., and Hansson, G. K. (2011) Progress and
440 challenges in translating the biology of atherosclerosis. *Nature* 473,
441 317–325.
442 (2) Lobatto, M. E., Calcagno, C., Millon, A., Senders, M. L., Fay, F.,
443 Robson, P. M., Ramachandran, S., Binderup, T., Paridaans, M. P.,
444 Sensarn, S., et al. (2015) Atherosclerotic Plaque Targeting Mechanism
445 of Long-Circulating Nanoparticles Established by Multimodal Imaging.
446 *ACS Nano* 9, 1837–1847.
447 (3) Melzer, S., Ankri, R., Fixler, D., and Tarnok, A. (2015) 447
448 Nanoparticle uptake by macrophages in vulnerable plaques for
449 atherosclerosis diagnosis. *J. Biophotonics* 8, 871.
450 (4) Seo, J. W., Baek, H., Mahakian, L. M., Kusunose, J., Hamzah, J.,
451 Ruoslahti, E., and Ferrara, K. W. (2014) (64)Cu-labeled LyP-1-
452 dendrimer for PET-CT imaging of atherosclerotic plaque. *Bioconjugate*
453 *Chem.* 25, 231–239.
454 (5) Kheiriloomoo, A., Kim, C. W., Seo, J. W., Kumar, S., Son, D. J.,
455 Gagnon, M. K., Ingham, E. S., Ferrara, K. W., and Jo, H. (2015) 455
456 Multifunctional Nanoparticles Facilitate Molecular Targeting and
457 miRNA Delivery to Inhibit Atherosclerosis in ApoE(−/−) Mice. 457
458 *ACS Nano* 9, 8885–8897.
459 (6) Couvreur, P. (2013) Nanoparticles in drug delivery: past, present 459
460 and future. *Adv. Drug Delivery Rev.* 65, 21–23.
461 (7) Wolfram, J., Shen, H., and Ferrari, M. (2015) Multistage vector 461
462 (MSV) therapeutics. *J. Controlled Release* 219, 406.
463 (8) Luk, B. T., Fang, R. H., and Zhang, L. (2012) Lipid- and 463
464 Polymer-Based Nanostructures for Cancer Theranostics. *Theranostics* 464
465 2, 1117–1126.
466 (9) Ryu, J. H., Lee, S., Son, S., Kim, S. H., Leary, J. F., Choi, K., and 466
467 Kwon, I. C. (2014) Theranostic nanoparticles for future personalized
468 medicine. *J. Controlled Release* 190, 477–484.
469 (10) Biswas, S., Kulkarni, J. A., Tam, Y. Y., Chem, S., Tam, Y. K., and 469
470 Cullis, P. (2015) *In Next generation magnetic lipid nanohybrids for*
471 *theranostics*, 250th ACS National Meeting, Fall 2015, Boston, MA, Aug
472 16–20, 2015; American Chemical Society, Washington, DC. 472
473 (11) von zur Muhlen, C., von Elverfeldt, D., Bassler, N., Neudorfer, 473
474 I., Steitz, B., Petri-Fink, A., Hofmann, H., Bode, C., and Peter, K. 474
475 (2007) Superparamagnetic iron oxide binding and uptake as imaged
476 by magnetic resonance is mediated by the integrin receptor Mac-1
477 (CD11b/CD18): Implications on imaging of atherosclerotic plaques. 477
478 *Atherosclerosis* 193, 102–111.
479 (12) Lobatto, M. E., Fuster, V., Fayad, Z. A., and Mulder, W. J. M. 479
480 (2011) Perspectives and opportunities for nanomedicine in the
481 management of atherosclerosis. *Nat. Rev. Drug Discovery* 10, 835–852. 481
482 (13) Zhao, X., Zhao, H., Chen, Z., and Lan, M. (2014) Ultrasmall 482
483 superparamagnetic iron oxide nanoparticles for magnetic resonance
484 imaging contrast agent. *J. Nanosci. Nanotechnol.* 14, 210–220. 484
485 (14) Taylor, R. M., Huber, D. L., Monson, T. C., Ali, M. S., Bisoffi, 485
486 M., and Sillerud, L. O. (2011) Multifunctional iron platinum stealth
487 immunomicelles: targeted detection of human prostate cancer cells
488 using both fluorescence and magnetic resonance imaging. *J. Nanopart.* 488
489 *Res.* 13, 4717–4729.
490 (15) Lemon, C. M., Karnas, E., Han, X., Bruns, O. T., Kempa, T. J., 490
491 Fukumura, D., Bawendi, M. G., Jain, R. K., Duda, D. G., and Nocera, 491
492 D. G. (2015) Micelle-Encapsulated Quantum Dot-Porphyrin
493 Assemblies as in Vivo Two-Photon Oxygen Sensors. *J. Am. Chem.* 493
494 *Soc.* 137, 9832–9842.
495 (16) Al-Jamal, W. T., and Kostarelos, K. (2011) Liposomes: from a 495
496 clinically established drug delivery system to a nanoparticle platform
497 for theranostic nanomedicine. *Acc. Chem. Res.* 44, 1094–1104. 497
498 (17) Al-Jamal, W. T., Al-Jamal, K. T., Bomans, P. H., Frederik, P. M., 498
499 Kostarelos, K. (2008) Functionalized-quantum-dot-liposome
500 hybrids as multimodal nanoparticles for cancer. *Small* 4, 1406–1415. 500
501 (18) Nie, S., Zhang, J., Martinez-Zaguilan, R., Sennoune, S., Hossen, 501
502 M. N., Lichtenstein, A. H., Cao, J., Meyerrose, G. E., Paone, R.,
503 Soontrapa, S., Fan, Z., and Wang, S. (2015) Detection of
504 atherosclerotic lesions and intimal macrophages using CD36-targeted
505 nanovesicles. *J. Controlled Release* 220, 61–70. 505

- 506 (19) Ekambaram, P., Abdul Hasan Sathali, A., and Priyanka, K.
507 (2012) Solid Lipid Nanoparticles: a review. *Sci. Rev. Chem. Commun. 2*,
508 80–102.
- 509 (20) Bae, K. H., Lee, J. Y., Park, T. G., and Nam, Y. S. (2013)
510 Optically Traceable Solid Lipid Nanoparticles Loaded with siRNA and
511 Paclitaxel for Synergistic Chemotherapy with In situ Imaging. *Adv.*
512 *Healthcare Mater. 2*, 576–584.
- 513 (21) Aimé, A., Beztsinna, N., Patwa, A., Pokolenko, A., Bestel, I., and
514 Barthélémy, P. (2013) Quantum Dot Lipid Oligonucleotide
515 Bioconjugates: Toward a New Anti-MicroRNA Nanoplatfrom.
516 *Bioconjugate Chem. 24*, 1345–1355.
- 517 (22) Luvino, D., Khiati, S., Oumzil, K., Rocchi, P., Camplo, M., and
518 Barthélémy, P. (2013) Efficient delivery of therapeutic small nucleic
519 acids to prostate cancer cells using ketal nucleoside lipid nanoparticles.
520 *J. Controlled Release 172*, 954–961.
- 521 (23) Immordino, M. L., Dosio, F., and Cattell, L. (2006) Stealth
522 liposomes: review of the basic science, rationale, and clinical
523 applications, existing and potential. *Int. J. Nanomedicine 1*, 297–315.
- 524 (24) Chabaud, P., Camplo, M., Payet, D., Serin, G., Moreau, L.,
525 Barthélémy, P., and Grinstaff, M. W. (2006) Cationic nucleoside lipids
526 for gene delivery. *Bioconjugate Chem. 17*, 466–472.
- 527 (25) Patel, D., Kell, A., Simard, B., Xiang, B., Lin, H. Y., and Tian, G.
528 (2011) The cell labeling efficacy, cytotoxicity and relaxivity of copper-
529 activated MRI/PET imaging contrast agents. *Biomaterials 32*, 1167–
530 1176.
- 531 (26) Guo, S., Shen, S., Wang, J., Wang, H., Li, M., Liu, Y., Hou, F.,
532 Liao, Y., and Bin, J. (2015) Detection of high-risk atherosclerotic
533 plaques with ultrasound molecular imaging of glycoprotein IIb/IIIa
534 receptor on activated platelets. *Theranostics 5*, 418–430.
- 535 (27) Lewis, D. R., Petersen, L. K., York, A. W., Zablocki, K. R.,
536 Joseph, L. B., Kholodovych, V., Prud'homme, R. K., Urich, K. E., and
537 Moghe, P. V. (2015) Sugar-based amphiphilic nanoparticles arrest
538 atherosclerosis in vivo. *Proc. Natl. Acad. Sci. U. S. A. 112*, 2693–2698.
- 539 (28) Sanchez-Gaytan, B. L., Fay, F., Lobatto, M. E., Tang, J., Ouimet,
540 M., Kim, Y. T., van der Staay, S. E. M., van Rijst, S. M., Priem, B.,
541 Zhang, L., Fisher, E. A., Moore, K. J., Langer, R., Fayad, Z. A., and
542 Mulder, W. J. M. (2015) HDL-Mimetic PLGA Nanoparticle To
543 Target Atherosclerosis Plaque Macrophages. *Bioconjugate Chem. 26*,
544 443–451.
- 545 (29) Rader, D. J., and Daugherty, A. (2008) Translating molecular
546 discoveries into new therapies for atherosclerosis. *Nature 451*, 904–
547 913.
- 548 (30) Arehart, E., Stitham, J., Asselbergs, F. W., Douville, K.,
549 MacKenzie, T., Fetalvero, K. M., Gleim, S., Kasza, Z., Rao, Y.,
550 Martel, L., Segel, S., Robb, J., Kaplan, A., Simons, M., Powell, R. J.,
551 Moore, J. H., Rimm, E. B., Martin, K. A., and Hwa, J. (2008)
552 Acceleration of Cardiovascular Disease by a Dysfunctional Prostacyclin
553 Receptor Mutation. *Circ. Res. 102*, 986–993.
- 554 (31) Arehart, E., Gleim, S., Kasza, Z., Fetalvero, K. M., Martin, K. A.,
555 and Hwa, J. (2007) Prostacyclin, Atherothrombosis, and Cardiovas-
556 cular Disease. *Curr. Med. Chem. 14*, 2161–2169.
- 557 (32) Kawabe, J.-I., Ushikubi, F., and Hasebe, N. (2010) Prostacyclin
558 in Vascular Diseases - Recent Insights and Future Perspectives. *Circ. J.*
559 *74*, 836–843.
- 560 (33) Jacobin-Valat, M. J., Laroche-Traineau, J., Lariviere, M., Mornet,
561 S., Sanchez, S., Biran, M., Lebaron, C., Boudon, J., Lacomme, S.,
562 Cérutti, M., and Clofent-Sanchez, G. (2015) Nanoparticles functional-
563 ised with an anti-platelet human antibody for in vivo detection of
564 atherosclerotic plaque by magnetic resonance imaging. *Nanomedicine*
565 *11*, 927–937.
- 566 (34) Roy, C. E., Kauss, T., Prevot, S., Barthélémy, P., and Gaudin, K.
567 (2015) Analysis of fatty acid samples by hydrophilic interaction liquid
568 chromatography and charged aerosol detector. *J. Chromatogr. A 1383*,
569 121–126.
- 570 (35) Oumzil, K., Khiati, S., Grinstaff, M. W., and Barthélémy, P.
571 (2011) Reduction-triggered delivery using nucleoside-lipid based
572 carriers possessing a cleavable PEG coating. *J. Controlled Release 151*,
573 123–30.
- (36) Khiati, S., Pierre, N., Andriamanarivo, S., Grinstaff, M. W., 574
Arazam, N., Nallet, F., Navailles, L., and Barthélémy, P. (2009) 575
Anionic Nucleotide-Lipids for In Vitro DNA Transfection. *Bio-* 576
conjugate Chem. 20, 1765–1772. 577